Medical Physics
The International Journal of Medical Physics Research and Practice

Experimental and Monte Carlo studies of fluence corrections for graphite calorimetry in low- and high-energy clinical proton beams

Ana Lourenço, Russell Thomas, Hugo Bouchard, Andrzej Kacperek, Vladimir Vondracek, Gary Royle, and Hugo Palmans

Citation: Medical Physics **43**, 4122 (2016); doi: 10.1118/1.4951733
View online: http://dx.doi.org/10.1118/1.4951733
View Table of Contents: http://scitation.aip.org/content/aapm/journal/medphys/43/7?ver=pdfcov
Published by the American Association of Physicists in Medicine

Experimental and Monte Carlo studies of fluence corrections for graphite calorimetry in low- and high-energy clinical proton beams

Ana Lourenço[a)]
Department of Medical Physics and Biomedical Engineering, University College London, London WC1E 6BT, United Kingdom and Division of Acoustics and Ionising Radiation, National Physical Laboratory, Teddington TW11 0LW, United Kingdom

Russell Thomas and Hugo Bouchard
Division of Acoustics and Ionising Radiation, National Physical Laboratory, Teddington TW11 0LW, United Kingdom

Andrzej Kacperek
National Eye Proton Therapy Centre, Clatterbridge Cancer Centre, Wirral CH63 4JY, United Kingdom

Vladimir Vondracek
Proton Therapy Center, Budinova 1a, Prague 8 CZ-180 00, Czech Republic

Gary Royle
Department of Medical Physics and Biomedical Engineering, University College London, London WC1E 6BT, United Kingdom

Hugo Palmans
Division of Acoustics and Ionising Radiation, National Physical Laboratory, Teddington TW11 0LW, United Kingdom and Medical Physics Group, EBG MedAustron GmbH, A-2700 Wiener Neustadt, Austria

(Received 11 December 2015; revised 4 April 2016; accepted for publication 10 May 2016; published 13 June 2016)

Purpose: The aim of this study was to determine fluence corrections necessary to convert absorbed dose to graphite, measured by graphite calorimetry, to absorbed dose to water. Fluence corrections were obtained from experiments and Monte Carlo simulations in low- and high-energy proton beams.
Methods: Fluence corrections were calculated to account for the difference in fluence between water and graphite at equivalent depths. Measurements were performed with narrow proton beams. Plane-parallel-plate ionization chambers with a large collecting area compared to the beam diameter were used to intercept the whole beam. High- and low-energy proton beams were provided by a scanning and double scattering delivery system, respectively. A mathematical formalism was established to relate fluence corrections derived from Monte Carlo simulations, using the FLUKA code [A. Ferrari *et al.*, "FLUKA: A multi-particle transport code," in CERN 2005-10, INFN/TC 05/11, SLAC-R-773 (2005) and T. T. Böhlen *et al.*, "The FLUKA Code: Developments and challenges for high energy and medical applications," Nucl. Data Sheets **120**, 211–214 (2014)], to partial fluence corrections measured experimentally.
Results: A good agreement was found between the partial fluence corrections derived by Monte Carlo simulations and those determined experimentally. For a high-energy beam of 180 MeV, the fluence corrections from Monte Carlo simulations were found to increase from 0.99 to 1.04 with depth. In the case of a low-energy beam of 60 MeV, the magnitude of fluence corrections was approximately 0.99 at all depths when calculated in the sensitive area of the chamber used in the experiments. Fluence correction calculations were also performed for a larger area and found to increase from 0.99 at the surface to 1.01 at greater depths.
Conclusions: Fluence corrections obtained experimentally are partial fluence corrections because they account for differences in the primary and part of the secondary particle fluence. A correction factor, $F(d)$, has been established to relate fluence corrections defined theoretically to partial fluence corrections derived experimentally. The findings presented here are also relevant to water and tissue-equivalent-plastic materials given their carbon content. [http://dx.doi.org/10.1118/1.4951733]

Key words: proton therapy, absolute dosimetry, graphite calorimetry, conversion factors, fluence corrections

1. INTRODUCTION

At present, a calibration service based on a primary-standard calorimeter for the direct determination of absorbed dose to water for proton beams does not exist.[3] Ion-chamber dosimetry under reference conditions is performed based on chambers calibrated in other modalities, for example, cobalt-60 beams. Consequently, the uncertainties are larger, 2.3% and 3.4% for protons and heavy-ion beams, respectively, when compared to a combined uncertainty of 1.5% for photon beams.[4]

A portable primary-standard level graphite calorimeter for light-ion beams was built at the National Physical Laboratory (NPL),[5] UK, based on earlier experience obtained with a small-body calorimeter.[6] This calorimeter will enable the provision of a direct absorbed dose-to-water calibration service. Users of this service would be the national eye Clatterbridge Cancer Centre (CCC), UK, and the two high-energy proton centers, currently under construction in the UK. Although graphite calorimetry has advantages,[7–10] the quantity measured is absorbed dose to graphite, D_g. Therefore, a conversion factor is necessary to determine absorbed dose to water, D_w.

The conversion factor for the determination of absorbed dose to water is the main source of uncertainty in graphite calorimetry. Dose to water and dose to graphite, at equivalent depths, are related by the water-to-graphite mass-stopping-power ratio and the fluence correction factor, k_{fl}. In proton beams, nonelastic nuclear interactions take place which decrease the primary beam fluence and produce secondary particles.[11] The difference between nonelastic nuclear interaction cross sections for different elements results in different attenuations of primary protons and different production rates of secondary particles. Consequently, the particle fluence present in water and graphite at equivalent depths will be different. This difference is corrected by the factor k_{fl}, which is determined from the charged particle fluence distributions in water and in graphite at scaled depths.[12]

Several studies have been performed to determine fluence corrections for graphite calorimetry in proton beams. Lühr *et al.*[13] determined fluence correction factors and stopping-power ratios for graphite, bone, and PMMA with the Monte Carlo code SHIELD-HIT10A for several light-ion beams including low- and high-energy proton beams. The authors showed that the correction was material, energy, and projectile particle-type dependent. They reported that fluence corrections for high-energy beams were approximately 5%. Palmans *et al.*[12] estimated fluence correction factors in a low-energy monoenergetic proton beam from an analytical model and simulations using five different Monte Carlo codes. Contributions from different types of charged particles were assessed, and it was shown that secondary particles should be included in calculations of fluence corrections. A comparison between numerical simulations and experimental data from water-to-graphite fluence corrections in light-ion beams was performed by Rossomme *et al.*[14] for a low-energy carbon-ion beam and by Palmans *et al.*[15] for a low-energy monoenergetic proton beam. Ding *et al.*[16] derived fluence corrections for electron beams using the EGS4 user-code BEAM for various plastic materials and compared their results to those from Kase *et al.*[17] and Thwaites.[18]

This study aims to present a novel method to determine fluence corrections experimentally, and to apply this methodology to low- and high-energy clinical proton beams. Fluence corrections were also obtained through Monte Carlo simulations, using the FLUKA code,[1,2] for comparison with the experiments. Experimental information was obtained from ionization chamber measurements of doses at depth in a water tank with and without graphite slabs upstream the front face of the water tank. One distinct advantage of this method, compared to earlier work,[15] is that only ionization chamber readings for water are required. A mathematical formalism which relates fluence corrections derived from Monte Carlo simulations to partial fluence corrections measured experimentally is presented.

2. THEORY

2.A. Relation between experimental and Monte Carlo calculated fluence corrections

A mathematical formalism is presented to relate fluence corrections calculated experimentally to those obtained from numerical simulations. The equations established here were employed to compute fluence corrections between water (w) and graphite (g). The term $K_A^{(n)}$ refers to a variable K, in a medium A, calculated using setup number n. The three different experimental setups under consideration are shown in Fig. 1. The quantities of interest are as follows:

1. Setup 1: dose to water in an homogeneous phantom of water, $D_w^{(1)}$;
2. Setup 2: dose to graphite in an homogeneous phantom of graphite, $D_g^{(2)}$;
3. Setup 3: dose to water in a phantom of water after passing through a thickness of graphite (t_g), $D_w^{(3)}$.

As derived by Palmans *et al.*,[12,19] dose to water, $D_w^{(1)}(z_{w-eq})$, and dose to graphite, $D_g^{(2)}(z_g)$, from a graphite calorimeter at equivalent depths, $z_{(eq)}$, are related by the water-to-graphite Bragg–Gray stopping-power ratio, $s_{w,g}^{BG}(\Phi_g)$, and the fluence correction factor, k_{fl},

$$D_w^{(1)}(z_{w-eq}) = D_g^{(2)}(z_g) \cdot s_{w,g}^{BG}(\Phi_g) \cdot k_{fl}. \quad (1)$$

A given depth in graphite is related to an equivalent depth in water by

$$z_{w-eq} = z_g \cdot \frac{r_{w,80}^{(1)}}{r_{g,80}^{(2)}}, \quad (2)$$

where $r_{w,80}^{(1)}$ and $r_{g,80}^{(2)}$ are depths in water and graphite, respectively, at which the dose drops to 80% of its maximum at the distal edge of the Bragg peak. There is evidence[20] that the 80% distal value of the Bragg peak corresponds to the depth reached by 50% of primary protons, i.e., protons which did not undergo nuclear interactions. This depth is approximately

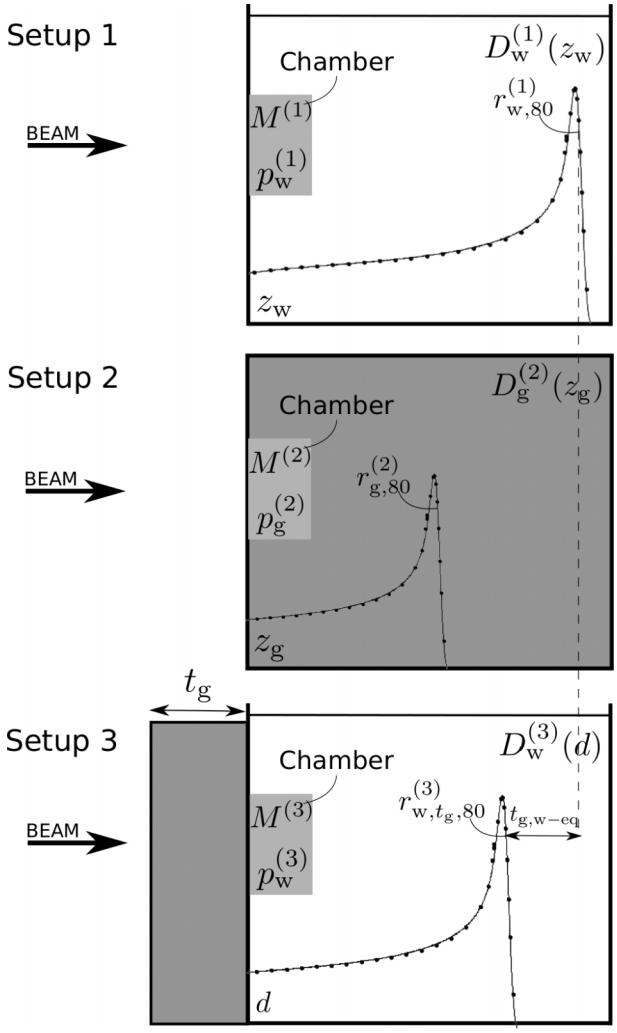

FIG. 1. Schematic representation of the three experimental setups considered. The gray color in setup 2 indicates a phantom composed of graphite while in setup 3 it depicts graphite slabs of variable thickness t_{g}. The phantoms shown in white are filled with water.

independent of the energy spread of incident beams with the same mean energy.[20]

Using Monte Carlo methods, Palmans *et al.*[12] calculated the fluence correction factor, $k_{\mathrm{fl,dose}}^{\mathrm{MC}}$, as a ratio of doses expressed as

$$k_{\mathrm{fl,dose}}^{\mathrm{MC}}(z_{\mathrm{w-eq}}) = \frac{D_{\mathrm{w}}^{(1)}(z_{\mathrm{w-eq}})}{D_{\mathrm{g}}^{(2)}(z_{\mathrm{g}}) \cdot s_{\mathrm{w,g}}^{\mathrm{BG}}(\Phi_{\mathrm{g}})}, \tag{3}$$

and the fluence correction factor, $k_{\mathrm{fl,fluence}}^{\mathrm{MC}}$, from fluence distributions differential in energy in water and graphite,

$$k_{\mathrm{fl,fluence}}^{\mathrm{MC}}(z_{\mathrm{w-eq}}) = \frac{\sum_i \left[\int_{E_{\mathrm{min},i}}^{E_{\mathrm{max},i}} \Phi_{E,\mathrm{w},i}^{(1)}(E) \cdot \left(\frac{S_i(E)}{\rho} \right)_{\mathrm{w}} \cdot \mathrm{dE} \right]}{\sum_i \left[\int_{E_{\mathrm{min},i}}^{E_{\mathrm{max},i}} \Phi_{E,\mathrm{g},i}^{(2)}(E) \cdot \left(\frac{S_i(E)}{\rho} \right)_{\mathrm{w}} \cdot \mathrm{dE} \right]}, \tag{4}$$

where i represents the charged particle types, $\Phi_E(E)$ the fluence differential in energy, and S/ρ the mass stopping-power. The influence of secondary electron transport was not considered. A detailed description of Eqs. (3) and (4) can be found in the work of Palmans *et al.*[12] In this work, cutoff energies for protons and heavier particles were set to 100 keV, with a typical continuous slowing down approximation (CSDA) range of 1.607×10^{-4} g cm^{-2} for protons in water.[21,22]

The IAEA TRS-398 Code of Practice[4] defines the fluence scaling factor, h_{pl}, to account for the difference in charged particle fluence between homogeneous phantoms of water and plastics. Palmans *et al.*[15] applied this definition to proton beams, and Rossomme *et al.*[14] to carbon-ion beams using setups 1 and 2. In this work, in order to derive fluence corrections by experiment, $k_{\mathrm{fl}}^{\mathrm{exp}}$, depth–dose curves were measured using setups 1 and 3. The latter is preferable to setup 2 which requires sampling sufficient data points across the experimental range in graphite; a time consuming approach due to the steepness of the Bragg peak and the need to manually change the graphite thickness. Furthermore, the ratio of ion chamber perturbation correction factors in water and graphite are not well known for proton therapy beams. For setups 1 and 3, it can be assumed that by always measuring in water there is little variation in the ratio of ion chamber perturbations.

A comparison between setups 1 and 3 should be made at a water-equivalent depth. For each slab, or set of slabs, an accurate value of the water-equivalent thickness (WET), $t_{\mathrm{g,w-eq}}$, was determined. Depth–dose measurements were made in water, with and without, graphite slabs upstream the front wall of the water phantom. For each slab or each combination of slabs used, the WET, $t_{\mathrm{g,w-eq}}$, was determined by the shift of the Bragg peak as shown in Fig. 1,

$$t_{\mathrm{g,w-eq}} = r_{\mathrm{w},80}^{(1)} - r_{\mathrm{w},t_{\mathrm{g}},80}^{(3)}. \tag{5}$$

In setup 1, and in keeping with the Bragg–Gray cavity theory, the dose $D_{\mathrm{w}}^{(1)}$ at a depth z_{w} is related to the ion chamber reading at the same depth, $M^{(1)}$ by,

$$D_{\mathrm{w}}^{(1)}(z_{\mathrm{w}}) = M^{(1)}(z_{\mathrm{w}}) \cdot \frac{W_{\mathrm{air}}/e}{m_{\mathrm{air}}} \cdot s_{\mathrm{w,air}}^{\mathrm{SA}}(\Phi_{\mathrm{w}}^{(1)}) \cdot p_{\mathrm{w}}^{(1)}(z_{\mathrm{w}}) \tag{6}$$

where m_{air} is the mass of air in the cavity, W_{air}/e is the average energy required to form an ion pair in air, $s_{\mathrm{w,air}}^{\mathrm{SA}}$ is the water-to-air Spencer–Attix stopping-power ratio, and $p_{\mathrm{w}}^{(1)}$ is the perturbation correction factor for the ionization chamber in water.

Similarly, in setup 3, the dose $D_{\mathrm{w}}^{(3)}$ at a depth in water d, for a graphite thickness t_{g} can be expressed as

$$D_{\mathrm{w}}^{(3)}(d,t_{\mathrm{g}}) = M^{(3)}(d,t_{\mathrm{g}}) \cdot \frac{W_{\mathrm{air}}/e}{m_{\mathrm{air}}} \cdot s_{\mathrm{w,air}}^{\mathrm{SA}}(\Phi_{\mathrm{w}}^{(3)}) \cdot p_{\mathrm{w}}^{(3)}(d,t_{\mathrm{g}}), \tag{7}$$

where $s_{\mathrm{w,air}}^{\mathrm{SA}}$ refers to a quantity $\Phi_{\mathrm{w}}^{(3)}$ that represents the fluence in water after passing through a layer of graphite, and $p_{\mathrm{w}}^{(3)}$ is the perturbation correction factor in water for the fluence $\Phi_{\mathrm{w}}^{(3)}$.

Depth in water is defined as $z_{\mathrm{w}} = d + t_{\mathrm{g,w-eq}}$, where d corresponds to an arbitrary depth in setup 3 and $d = 0$ at the interface between graphite and water. The ratio of ion chamber readings $M^{(1)}$ and $M^{(3)}$ can be obtained from combining Eqs. (6) and (7),

$$\frac{M^{(1)}(z_w)}{M^{(3)}(d,t_g)} = \frac{D_w^{(1)}(z_w)}{D_w^{(3)}(d,t_g)} \cdot \frac{W_{air}/e}{W_{air}/e} \cdot \frac{s_{w,air}^{SA}(\Phi_w^{(3)})}{s_{w,air}^{SA}(\Phi_w^{(1)})} \cdot \frac{p_w^{(3)}(d,t_g)}{p_w^{(1)}(z_w)}. \quad (8)$$

We assume the following: (i) the difference in chamber perturbation between setups 1 and 3 is negligible, $p_w^{(3)}(d,t_g) \approx p_w^{(1)}(z_w)$, (ii) the stopping-power ratio for $\Phi_w^{(3)}$ and $\Phi_w^{(1)}$ is equal, $s_{w,air}^{SA}(\Phi_w^{(3)}) \approx s_{w,air}^{SA}(\Phi_w^{(1)})$, and (iii) the variation of W_{air}/e between the two setups is negligible since the spectra are marginally different. The slow variation of the perturbation correction factors with energy[15,23] and the slow variation of the water-to-air stopping-power ratios with energy[21] support the first two assumptions. Furthermore, the validity of the assumptions described above was verified by Monte Carlo leading to an estimate of the maximum error smaller than 0.1%. Model data from Grosswendt and Baek[24] were used to calculate the variation of W_{air}/e between setups 1 and 3.

Dose in setup 3, $D_w^{(3)}(d,t_g) = \sum_i \left[\int_0^{E_{max,i}} \Phi_{E,w,i}^{(3)}(E) \cdot (S_i(E)/\rho)_w \cdot dE\right]$, is related with dose in setup 2, $D_g^{(2)}(z_g) = \sum_i \left[\int_0^{E_{max,i}} \Phi_{E,g,i}^{(2)}(E) \cdot (S_i(E)/\rho)_g \cdot dE\right]$, by the water-to-graphite stopping-power ratio $s_{w,g}^{BG}(\Phi_g)$ and a correction factor $F(d)$ that accounts for the difference in fluence between the setups, $D_w^{(3)}(d,t_g) = D_g^{(2)}(z_g) \cdot s_{w,g}^{BG}(\Phi_g) \cdot F(d)$, where

$$s_{w,g}^{BG}(\Phi_g) = \frac{\sum_i \left[\int_{E_{min,i}}^{E_{max,i}} \Phi_{E,g,i}^{(2)}(E) \cdot \left(\frac{S_i(E)}{\rho}\right)_w \cdot dE\right]}{\sum_i \left[\int_{E_{min,i}}^{E_{max,i}} \Phi_{E,g,i}^{(2)}(E) \cdot \left(\frac{S_i(E)}{\rho}\right)_g \cdot dE\right]}, \quad (9)$$

$$F(d) = \frac{\sum_i \left[\int_{E_{min,i}}^{E_{max,i}} \Phi_{E,w,i}^{(3)}(E) \cdot \left(\frac{S_i(E)}{\rho}\right)_w \cdot dE\right]}{\sum_i \left[\int_{E_{min,i}}^{E_{max,i}} \Phi_{E,g,i}^{(2)}(E) \cdot \left(\frac{S_i(E)}{\rho}\right)_w \cdot dE\right]}. \quad (10)$$

Thus, considering the assumptions described above, Eq. (8) can be expressed as,

$$\frac{M^{(1)}(z_w)}{M^{(3)}(d,t_g)} \approx \frac{D_w^{(1)}(z_w)}{D_g^{(2)}(z_g) \cdot s_{w,g}^{BG}(\Phi_g) \cdot F(d)} \approx \frac{k_{fl,dose}}{F(d)}. \quad (11)$$

Consequently, the measurement ratio is related to the total fluence correction factor, from Eq. (3), by a correction factor $F(d)$. Therefore, in keeping with Eq. (3), the total fluence correction factor can be calculated experimentally by

$$k_{fl}^{exp}(t_{g,w-eq}) \approx \frac{M^{(1)}(z_w)}{M^{(3)}(d,t_g)} \cdot F(d) \approx k_{fl,partial}^{exp} \cdot F(d). \quad (12)$$

Accordingly, the ratio of ion chamber readings from setups 1 and 3 represents a partial fluence correction factor because it accounts for differences in the primary and part of the secondary particle fluence. For the conversion of dose to graphite to dose to water, three main particles contribute to the fluence correction factor: primary protons, secondary protons, and alpha particles.[12] In FLUKA,[1,2] for incident proton energies of 60 and 200 MeV, in a proton-^{16}O collision, the average emission energies of alpha particles are 5.0 and 6.8 MeV and their corresponding CSDA ranges in water are 0.04 and 0.06 mm, respectively.[21] The range values are similar for proton-^{12}C collisions. These results are consistent with ICRU Report 63 data,[25] where for the same incident proton energies and type of collision, the average emission energies of alpha particles are 5.8 and 9.8 MeV, respectively. In keeping with ICRU Report 63,[25] uncertainties for total nonelastic cross sections and angle-integrated production cross sections for secondary particles are 5%–10% and 20%–30%, respectively, which could explain the differences between the models. The range of alpha particles indicate that particles generated in the slab of graphite, t_g, do not have enough energy to penetrate the chamber wall. The same applies to a fraction of secondary protons with low-energy, while high-energy secondary protons do reach the chambers cavity and are thus accounted in the partial fluence correction factor. Therefore, the measurement ratio represents a partial fluence correction factor,

$$k_{fl,partial}^{exp}(t_{g,w-eq}) \approx \frac{M^{(1)}(z_w)}{M^{(3)}(d,t_g)}, \quad (13)$$

and from Monte Carlo methods,

$$k_{fl,partial}^{MC}(t_{g,w-eq}) \approx \frac{D_w^{(1)}(z_w)}{D_w^{(3)}(d,t_g)}. \quad (14)$$

Assuming that the change in fluence from the surface to the measurement point is not different from setups 1 and 3, then $k_{fl,partial}$ for a specific $t_{g,w-eq}$ is the same value at every depth d and a mean value can be derived for N depths experimentally, expressed as

$$k_{fl,partial}^{exp}(t_{g,w-eq}) \approx \frac{1}{N} \sum_{j=1}^{N} \frac{M^{(1)}(z_w)}{M^{(3)}(d_j,t_g)}. \quad (15)$$

Also, using Monte Carlo methods,

$$k_{fl,partial}^{MC}(t_{g,w-eq}) \approx \frac{1}{N} \sum_{j=1}^{N} \frac{D_w^{(1)}(z_w)}{D_w^{(3)}(d_j,t_g)}. \quad (16)$$

This has been verified with Monte Carlo simulations and it avoids systematic errors. For each slab of graphite with thickness t_g tested experimentally, its water-equivalent thickness was calculated from Eq. (5). The ratio between water and graphite–water ionization readings was calculated at equivalent depths and a mean value was computed to represent $k_{fl,partial}^{exp}$ for a given slab t_g of graphite.

3. MATERIALS AND METHODS

3.A. Measurements

Measurements were performed at two separate clinical sites: the 60 MeV proton cyclotron at the Clatterbridge Cancer Centre (CCC), UK and the 226 MeV proton cyclotron at the PTC Czech Proton Therapy Centre (PTC Czech), using a beam of 180 MeV. Narrow beams were used without any range modulation. In the CCC beam, a collimator of 4 mm diameter was used, whereas in the case of the PTC Czech beam, a single spot was used. A PTW type 7862

transmission chamber was placed in front of the beam exit for monitoring purposes. A water phantom with an entrance window of 3.7 mm WET of PMMA was placed in front of the beam exit with the phantom surface aligned with the isocentre. Low-energy beam measurements were performed using a PTW 34001 Roos chamber with a sensitive diameter of 15 mm. High-energy beam measurements were carried out with a PTW 34070 Bragg peak chamber with sensitive diameter of 81.6 mm. The volume of both chambers was large in comparison to the beams diameter to ensure that all particles were intercepted. Since measurements were acquired for a laterally integrated fluence, there was no correction required for the inverse square law. The chambers were kept at a constant source-to-detector distance, SDD, in order to avoid corrections for the divergence of the beam. The water phantom was moved toward the gantry by a moving platform in order to vary the amount of water in front of the chamber. Measurements were repeated with graphite plates of variable thicknesses attached to the front window of the water tank.

3.B. Monte Carlo simulations

All the Monte Carlo simulations described in this work were performed with the FLUKA-2011.2c.2 code.[1,2] The fluence correction factor was computed using three approaches based on the following: dose thus establishing $k^{\mathrm{MC}}_{\mathrm{fl,dose}}$ from Eq. (3), fluence thus obtaining $k^{\mathrm{MC}}_{\mathrm{fl,fluence}}$ from Eq. (4), and partial fluence where $k^{\mathrm{MC}}_{\mathrm{fl,partial}}$ is derived from Eq. (16). For the dose and fluence approaches, measurements were performed in a pure water and graphite phantoms whereas in the case of the partial fluence method measurements were performed in a water phantom.

The entire geometry of the CCC scattering beam line was simulated as described in Refs. 26–28. The PTC Czech beam line configuration was not considered in the numerical simulations because it consists of a scanning system and therefore the influence of the beam line geometry on the calculation of the fluence correction factor is negligible.[14]

Depth–dose distributions and fluence differential in energy were simulated for the 60 MeV beam and for the 180 MeV beam in cylindrical phantoms of water ($\rho = 1.0$ g cm^{-3}) and graphite ($\rho = 1.8$ g cm^{-3}). The default card HADROTHErapy was activated with a delta-ray production set to infinite threshold such that delta-ray production was not considered in the simulations. The most energetic secondary electrons have a short range of <1 mm and therefore all energy transferred to electrons can be regarded as absorbed locally. Full transport of light- and heavy-ions was included. For the CCC beam simulations, transport of neutrons was not considered because these particles are mainly generated in the materials of the beam line and neutron dose has been reported to be less than 0.1% of the treatment dose.[28] CCC beam simulations were performed on cylindrical phantoms of 10 cm radius and 3.5 cm thickness. The absorbed doses were scored in 0.01 cm bins. For the calculation of $k^{\mathrm{MC}}_{\mathrm{fl,fluence}}$ and $k^{\mathrm{MC}}_{\mathrm{fl,dose}}$, the phantom was positioned with its surface at the isocentric plane (7 cm from the collimator exit). For each material, 5×10^8 primary particles were simulated. PTC Czech beam simulations were performed in a cylindrical phantom of 10 cm radius and 26 cm thickness. Absorbed doses for the latter were also scored in 0.01 cm bins and for each material 5×10^6 primary particles were simulated. Fluence differential in energy was scored in 0.1 cm thick slabs throughout the phantoms. Absorbed doses and fluences differential in energy were also scored in smaller volumes, equal to the sensitive area as the chambers used in the experiments.

In order to compute $k^{\mathrm{MC}}_{\mathrm{fl,partial}}$, absorbed doses were scored in the water phantom of setup 1 and compared to those from setup 3. Although during experiments the SDD was kept constant, it is significantly more efficient to perform Monte Carlo simulations with a constant source-to-surface distance (SSD). The latter only requires a single simulation to calculate dose with depth, whereas SDD setup requires a simulation for each depth. Consequently, SDD values were derived from SSD values as follows. $D^{\mathrm{SSD}}(z_{\mathrm{w}}, x_k)$ is the depth–dose curve obtained with SSD constant and $D^{\mathrm{SDD}}(z_{\mathrm{w}}, x_k)$ is the depth–dose curve obtained with SDD constant. In both situations, dose is a function of z_{w}, which is the depth in water, and x_k, which is a discrete variable that corresponds to the distance from the phantom surface to the reference plane (for which $x_k = 0$). For the setup with SSD constant, $x_k = 0$, and for the setup with SDD constant, $z_{\mathrm{w}} = x_k$. $D^{\mathrm{SDD}}(z_{\mathrm{w}}, x_k)$ was calculated at a discrete set of x_k values and a correction $C(z_{\mathrm{w}})$ was calculated to derive $D^{\mathrm{SDD}}(z_{\mathrm{w}}, x(k))$, where $x(k)$ represents a continuous variable, therefore,

$$D^{\mathrm{SDD}}(z_{\mathrm{w}},x(k)) \approx D^{\mathrm{SSD}}(z_{\mathrm{w}},0)\cdot C(z_{\mathrm{w}}), \tag{17}$$

where $C(z_{\mathrm{w}}) = D^{\mathrm{SDD}}(z_{\mathrm{w}},x_k)/D^{\mathrm{SSD}}(z_{\mathrm{w}},0)$. A cubic spline was fitted to $C(z_{\mathrm{w}})$ to obtain a continuous correction for all values z_{w}. Figure 2 shows the calculated ratio of $D^{\mathrm{SDD}}(z_{\mathrm{w}}, x_k)$ and $D^{\mathrm{SSD}}(z_{\mathrm{w}},0)$. For the PTC Czech beam the correction is very small, therefore, real depth–dose curves were calculated where the SSD was constant. For the CCC beam, the primary protons scattered at low angles, by the collimator edges, increase with decreasing collimator diameter.[28] Therefore, the beam size used was such that the contribution from the protons scattered at low angles was not negligible[28] and a correction was applied for the derivation of SDD from SSD.

3.C. Assessing uncertainties

Uncertainties were calculated as the standard deviation of the mean of repeated observations.[29] The sources of experimental uncertainties to determine $k^{\mathrm{exp}}_{\mathrm{fl,partial}}$ are presented in Table I for the measurements performed with the PTC Czech and the CCC beams. All uncertainties are expressed as relative standard uncertainties. The overall uncertainty is quoted to 1σ and was calculated by combining type A and B uncertainties in quadrature.[29] Type A and type B uncertainties were determined following the guidelines of the *Guide to the Expression of Uncertainty in Measurement* (GUM).[29]

The repeatability was considered as type A and the uncertainty in temperature, pressure, and standard deviation of the mean value of $k^{\mathrm{exp}}_{\mathrm{fl,partial}}$ with depth as type B. The

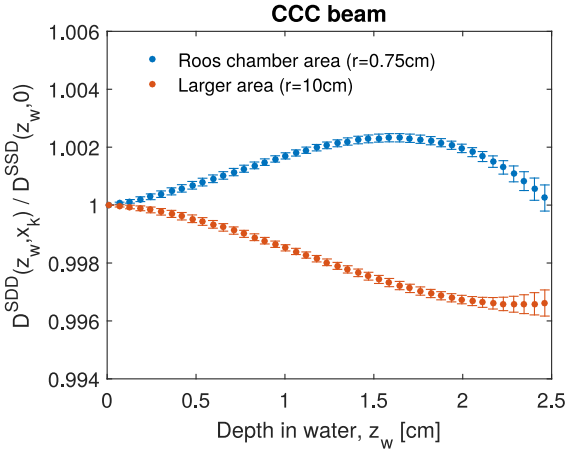

(a)

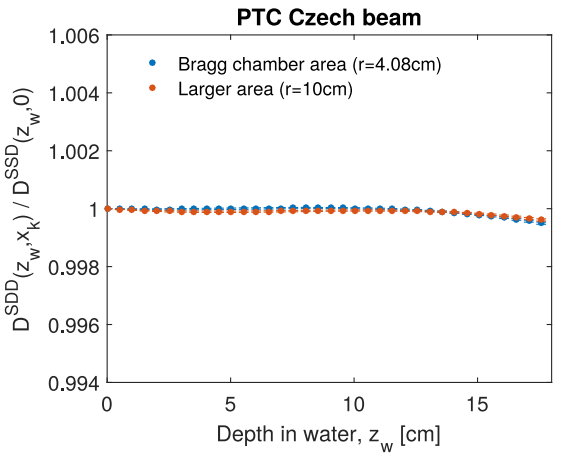

(b)

FIG. 2. Correction for the derivation of SDD from SSD for (a) the CCC beam and (b) the PTC Czech beam. The correction for the PTC Czech beam is very small.

same type of electrometer was used and thus for a given ratio of two readings, for example, standard chamber/monitor chamber, any type B uncertainty related to the electrometer was correlated and canceled out. The same applies to ion recombination corrections. Uncorrelated uncertainties, such as fluctuations and drifts, were considered negligible. For the PTC Czech experiments, variations in chamber position were also considered. During the experiments, the water pressure exerted on the Bragg chamber when the water phantom was moving resulted in an uncertainty in chamber position. This was because the chamber support was not suitable to accommodate a chamber of that size. Variations in chamber position were estimated based on position checks performed in the experiments.

It was more challenging to estimate Type B uncertainties in the Monte Carlo simulations than type A. Type B uncertainties include propagation of uncertainties from stopping-power data, material data, and interaction cross sections. For the energy range of 10–10^6 MeV, uncertainties in the stopping powers for elemental materials are smaller than 1%. In the low-energy region, uncertainties become as large as 5%–25%.[21] Material-data uncertainties include uncertainties in stopping powers and mean excitation energy (I-values). Nuclear data files can vary depending on the models implemented in a given Monte Carlo code and, at present, estimates of these type of uncertainties are not provided. However, in keeping with ICRU Report 63 (Ref. 25) uncertainties for total nonelastic cross sections and angle-integrated production cross sections for secondary particles are 5%–10% and 20%–30%, respectively. Type A uncertainties for the fluence correction factor computed by numerical simulations were below 0.2%. Uncertainties become larger when approaching the depth of the Bragg peak because positioning in depth becomes very critical due to the steep gradient. Therefore, those points were not considered in the calculation of the fluence correction factor.

4. RESULTS AND DISCUSSION

4.A. Depth–dose curves

In the experiments, laterally integrated measurements were performed in a narrow beam. The contribution of particles scattered outside the sensitive area of the chambers was evaluated using Monte Carlo simulations. The ratio between the energy deposited inside the chamber sensitive area and the energy deposited in a larger area was calculated and the results are shown in Fig. 3 for water and graphite.

For the PTC Czech beam, the ratio is very close to unity for primary protons because the deflection of the primary beam is small. Secondary protons, generated from nonelastic nuclear interactions, emerge with larger angles with respect to the

TABLE I. Experimental relative standard uncertainties for the PTC Czech and CCC beams.

Beam	PTC Czech		CCC	
Source of uncertainty	Type A (%)	Type B (%)	Type A (%)	Type B (%)
Repeatability	0.03	—	0.65	—
Temperature	—	0.05	—	0.05
Pressure	—	0.05	—	0.05
$s_{\overline{k^{exp}_{fl,partial}}}$	—	0.42	—	0.30
Variations in chamber position	—	0.79	N/A	N/A
Total	0.030	0.898	0.650	0.308
Overall (%)	0.9		0.7	

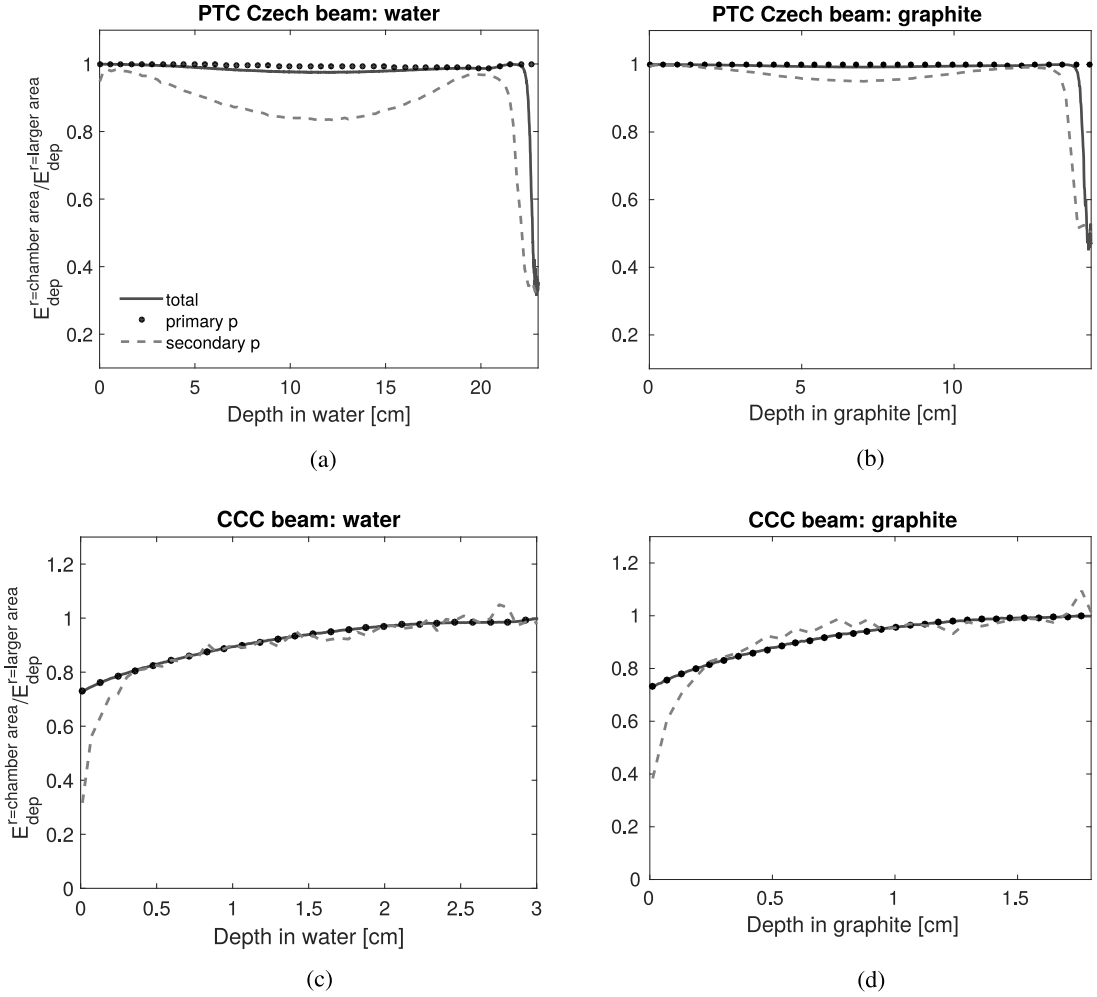

FIG. 3. Ratio between energy deposited inside the area of the chambers and energy deposited in a larger area. The graphs represent ratio of the total energy and energy due to the contribution of primary and secondary protons in water (left) and graphite (right).

incident proton direction and thus escape the sensitive area of the chamber. Accordingly, their contribution is not taken into account. Furthermore, water contains free hydrogen with which the projectile protons can undergo elastic collisions and produce secondary protons with larger scatter angles. The maximum total energy loss occurs in the build-up region and amounts to 2.5% and 0.8% for water and graphite, respectively. In addition, for graphite, the lateral projected range is shorter because its density is higher than that of water.

For the CCC beam, primary protons were scattered at low angles from the edges of the collimator and thus approximately 30% of the primary protons were not detected inside the area of the chamber.

The experimental depth–dose distribution in water, acquired with the PTC Czech beam, is compared with Monte Carlo simulations in Fig. 4. The WET of the front window of the water phantom and the water-equivalent-window thickness of the chambers were considered when defining the depths at which experimental measurements were carried out. Curves were normalized to unity at the entrance because chamber readings were expressed in units of Coulomb (C) and absorbed doses from Monte Carlo simulations were in units of Gray (Gy). Numerical simulations were tuned for 62.5 MeV at the source and 180 MeV, assuming energy spreads of $\sigma = 0.28$ MeV and 0.9 MeV for the CCC and PTC Czech beams, respectively.

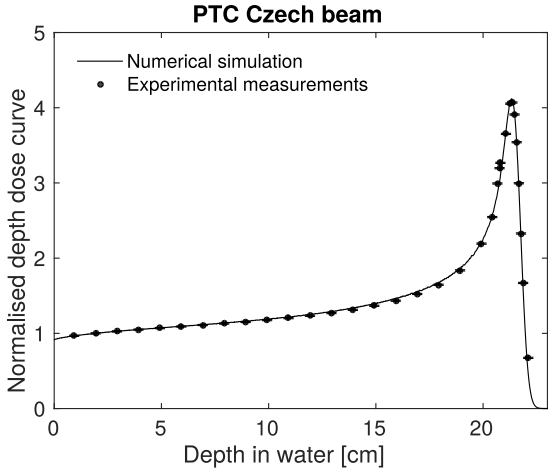

FIG. 4. Experimental and Monte Carlo depth–dose curves in water for the 180 MeV PTC Czech beam. Similar results were found for the 60 MeV CCC beam.

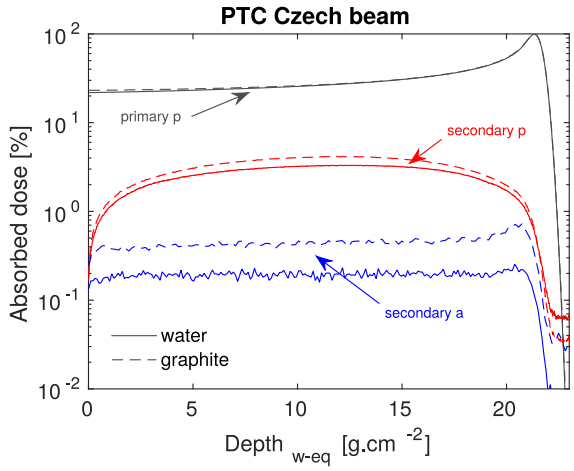

FIG. 5. Monte Carlo simulations of the absorbed dose curves as a function of depth for the PTC Czech beam in water (straight line) and graphite (dashed line). The graph shows the contribution of each particle in a percentage of absorbed dose (p = protons and a = alphas). Similar results were found for the CCC beam.

4.B. Dose from primary and secondary particles

The main three particle types that contribute to the fluence correction factor between water and graphite are primary protons, secondary protons, and alpha particles.[12] Figure 5 shows the contributions of these particles. The major contribution to the total dose stems from primary and secondary protons. The contribution of secondary particles is higher in graphite than in water due to a larger total nonelastic nuclear interaction cross section per atomic mass.[4] Particles scored for the calculation of the fluence correction factor were primary and secondary protons, alphas, ^{3}He ions, deuterons, and tritons.

4.C. Fluence corrections

4.C.1. PTC Czech beam

The fluence correction results for the PTC Czech beam as derived from the fluence and dose based methods are presented in Fig. 6. The quantities of interest were calculated in an area equal to the sensitive area of the chamber used experimentally. A calculation of fluence corrections in a larger area was also performed to account for particles that scatter outside the sensitive area of the chamber. Primary protons that undergo elastic nuclear interactions were considered as primary particles and in a p-H elastic collision, the largest energy proton was considered as primary. At the surface (depth = 0 cm), primary proton fluence is the same in both phantoms and the ratio of the fluences in water and graphite increases gradually with depth. This is because more primary particles are removed from the beam in graphite than in water at equivalent depths. To illustrate the effect of elastic nuclear interactions, two curves for primary protons are shown in Fig. 6(b), representing simulations where the elastic nuclear interactions were included and switched off by setting the energy threshold for these interactions very high. Primary protons which are elastic scattered have lower energy and

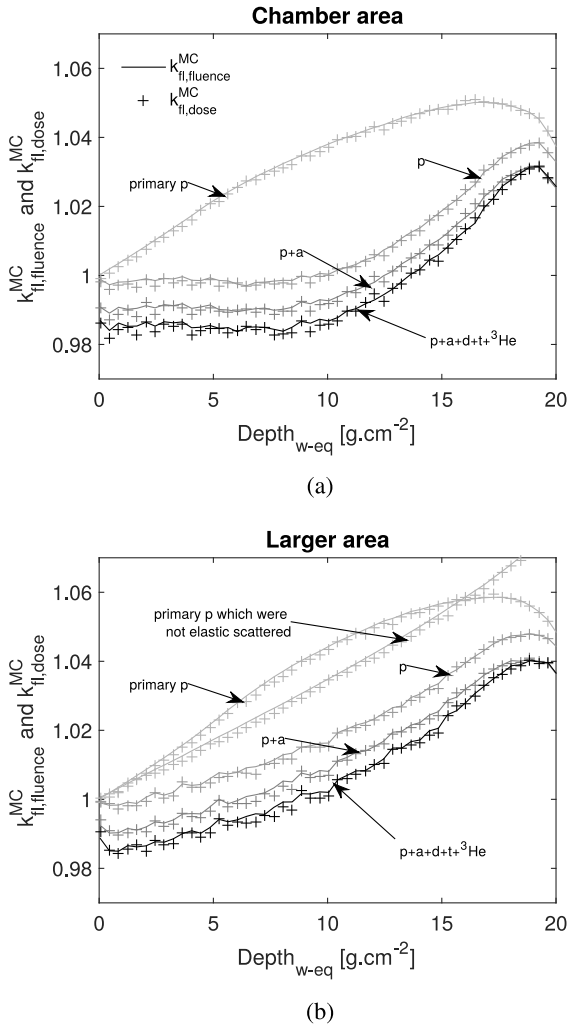

FIG. 6. Monte Carlo simulations of the fluence correction factor between water and graphite for the PTC Czech beam. Straight lines represent the fluence method [Eq. (4)] and crosses represent the dose method [Eq. (3)], (a) inside the area of the Bragg peak chamber and (b) in a larger area. The curves indicate the contributions of primary and secondary particles (primary p = primary protons, p = primary and secondary protons, a = alphas, d = deuterons, t = tritons, and ^{3}He ions).

larger scattering angles; therefore, their contribution is larger in the plateau region. Primary protons that are not elastic scattered have larger ranges and their contribution is larger in the Bragg peak region.

The contribution of secondary particles is different in water and in graphite, and these differences become apparent as soon as the secondary particles are produced at the surface. The difference of 1% at the surface can be mainly attributed to the contribution of alpha particles as can be seen in Fig. 5. Most of these particles travel a certain distance in the direction of the incident particles. However, given their very short range, close to the surface there is already a difference between the alpha fluence in water and graphite. As is shown in Fig. 5, the dose contribution due to alpha particles is higher in graphite than in water because the production cross section of these particles per atomic mass is larger for graphite than for water. This is consistent with data from ICRU Report 63,[25] where for

an 180 MeV proton beam, the alpha production cross section is approximately 25% larger in graphite than in water.

When all charged particles are considered, the fluence correction factor increases from 0.99 to 1.04 with depth. The results presented here are in agreement with the previous work performed by Lühr *et al.*[13] who found fluence corrections to be of the order of 5% in depth for high-energy proton beams using SHIELD-HIT10A Monte Carlo code. At larger depths, the energy deposition from secondary particles becomes negligible in comparison with the energy deposition from primaries and all the curves converge to the value obtained for primary particles. As illustrated in Fig. 3, secondary protons escape the collecting area of the chamber and this affects the fluence corrections. This difference is about 1% in the build-up region and is in agreement with the results shown in Figs. 3 and 6.

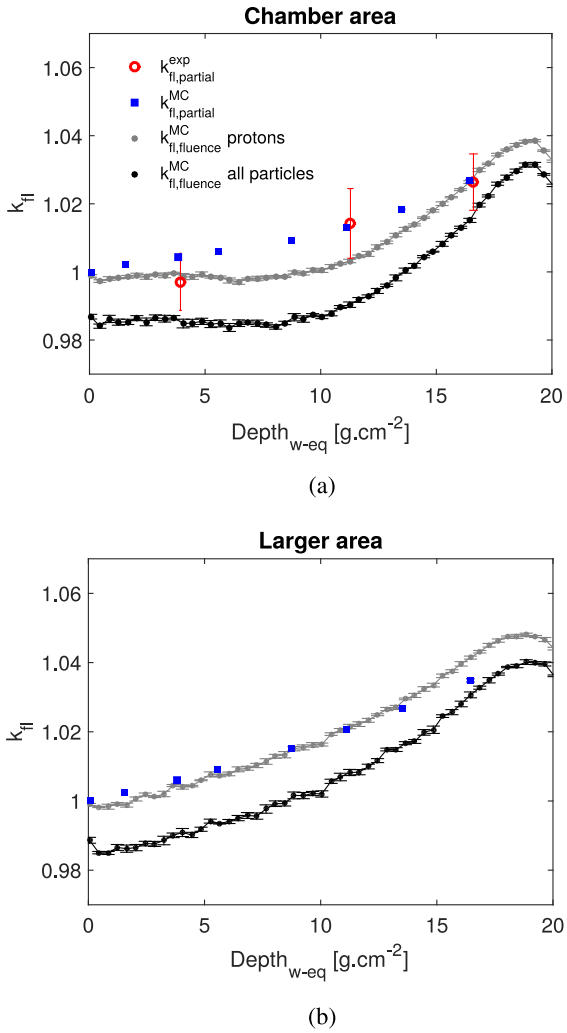

FIG. 7. Comparison between numerical simulations and experimental data of the fluence correction factor between water and graphite for the PTC Czech beam. Open circles represent the values of $k_{fl,partial}^{exp}$ calculated experimentally [refer to Eq. (15)], squares represent the values of $k_{fl,partial}^{MC}$ calculated using Monte Carlo methods [Eq. (16)], and solid circles represent the values of $k_{fl,fluence}^{MC}$ [refer to Eq. (4)] when taking into account the proton spectra, primary, and secondary particles, in gray, and all charged particles spectra in black; (a) inside the area of the Bragg peak chamber and (b) in a larger area.

For simplification and due to the good agreement between fluence method and dose method, the data of the latter have been excluded from the graphs presented in Fig. 7. A comparison between experimental data and numerical simulations of the fluence correction factor is shown in Fig. 7. The $k_{fl,partial}^{MC}$ factor was computed to simulate the experimental setup by Monte Carlo and to study the variation of the fluence correction factor at depth, d, for a specific thickness of graphite, t_g. In the numerical simulations, absorbed doses were scored for setup 1 and compared to absorbed doses in water from setup 3. The latter were simulated to have the same thickness and density of those used in the experiments, along with other thicknesses to obtain a more complete data set. For each slab of graphite with thickness t_g tested, its WET was calculated from the difference in ranges and the ratio between water and graphite–water absorbed dose curves was calculated at equivalent depths. For each slab of graphite, the fluence correction factor was found to be constant as a function of depth. Its variation was estimated to be 0.8% due to the statistics of the Monte Carlo simulations. When $k_{fl,partial}^{MC}$ is calculated in an area equal to the sensitive area of the chamber, the variation of $k_{fl,partial}^{MC}$ with depth increases for thicker slabs of t_g due to the difference in scattering between water and graphite. A mean value was computed to represent $k_{fl,partial}^{MC}$ as a function of WET, in keeping with Eq. (16). Figure 7 shows that $k_{fl,partial}^{exp}$ follows the same trend as $k_{fl,partial}^{MC}$. The ratio of ion chamber readings from setups 1 and 3, determined experimentally, and a ratio of doses from setups 1 and 3, calculated using Monte Carlo methods, represent a partial fluence correction factor that accounts for differences of primary and secondary proton spectra. As defined by Eq. (12), the partial fluence correction is related to the fluence correction factor, when accounting all charged particles, by the factor $F(d)$. The range of alpha particles is very short and the ones produced in the slab of graphite, t_g, do not penetrate the water phantom in setup 3. Consequently their contribution is not accounted for in the expression of $k_{fl,partial}^{MC}$. All alpha particles detected in the chamber cavity were generated within the chamber geometry (wall and cavity). Therefore, for a given proton fluence, the same amount of alpha particles will be observed in the cavity irrespective of the material of the phantom is. The results show that $F(d)$ varies from 0.98 to 1.00 at depth. In order to quantify $F(d)$ experimentally, an alternative detector such as a thin-window ion chamber detector could be used to sample the generated alpha particles contribution. Future work will focus on measuring $F(d)$ experimentally.

4.C.2. CCC beam

The results from the fluence and dose based methods are presented in Fig. 8 for the CCC beam. Quantities of interest were calculated in a volume with a sensitive area identical to that of the Roos ion chamber and were also scored in a larger area to study the contribution of particles that scatter outside the effective area of the chamber.

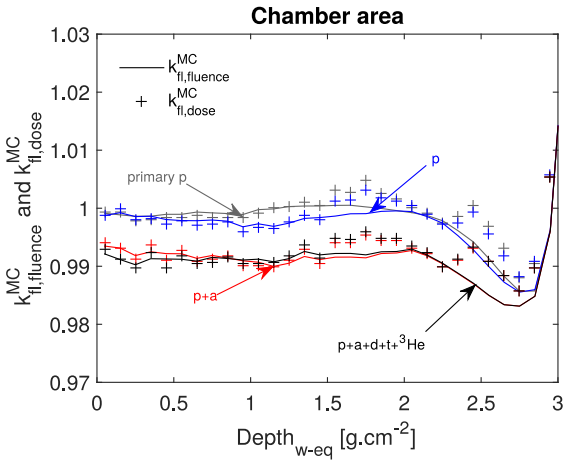

(a)

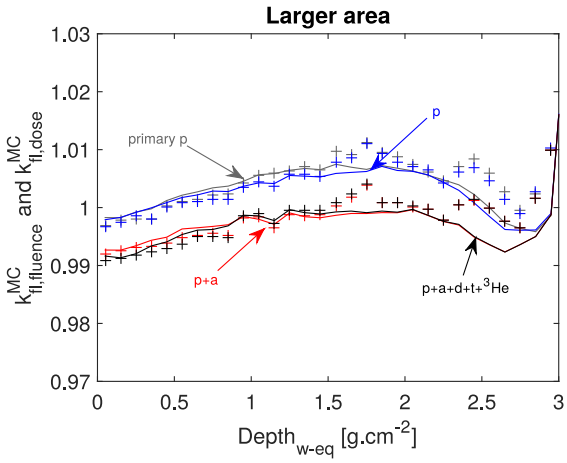

(b)

FIG. 8. Monte Carlo simulations of the fluence correction factor between water and graphite for the CCC beam. The solid lines represent the fluence method [Eq. (4)] and the crosses represent the dose based method [Eq. (3)], (a) inside the area of the Roos chamber and (b) in a larger area. The contributions of primary protons, primary and secondary protons, protons and alpha particles, and all charged particles are depicted in gray, blue, red, and black, respectively.

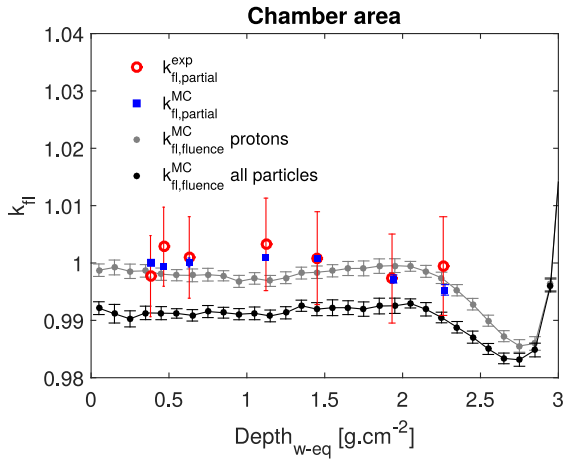

(a)

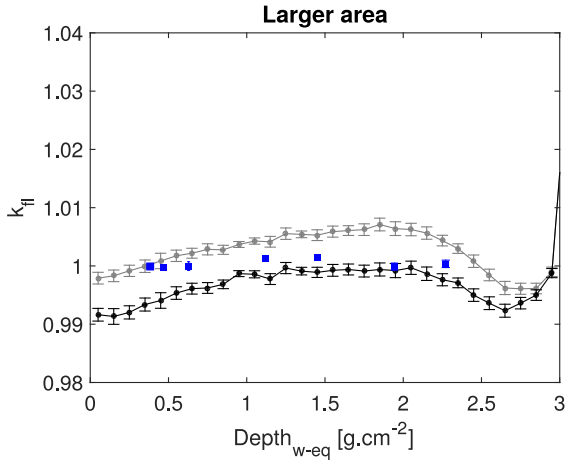

(b)

FIG. 9. Comparison between numerical simulations and experimental data of the fluence correction factor for the CCC beam. Open circles represent the values of $k^{exp}_{fl,partial}$ calculated experimentally [Eq. (15)], squares represent the values of $k^{MC}_{fl,partial}$ calculated using Monte Carlo methods [Eq. (16)], and solid circles represent the values of $k^{MC}_{fl,fluence}$ [Eq. (4)] when taking into account the proton spectra, primary and secondary protons, in gray, and all charged particles spectra in black; (a) inside the area of the Roos chamber and (b) in a larger area.

The fluence corrections calculated in this work are in agreement with those of Palmans *et al.*[12] The statistical Monte Carlo noise between the fluence and dose models is due to the scattering delivery system whose main disadvantage is the loss of a significant number of primary protons at the collimator exit. This is especially pronounced when small fields are employed as only about 3% of the protons impinging the first scattering foil are used for treatment.[30] The magnitude of the fluence correction factor, when accounting for all charged particle spectra, is approximately 0.99 at all depths inside the chamber area. When considering a larger area, it increases from 0.99 to 1.01 with depth.

A comparison between experimental data and numerical simulations of the fluence correction factor is shown in Fig. 9. A good agreement was found between partial fluence corrections measured in the experiments ($k^{exp}_{fl,partial}$), and those derived using Monte Carlo methods ($k^{MC}_{fl,partial}$). Partial fluence corrections ($k_{fl,partial}$) are related with fluence corrections defined by theory ($k^{MC}_{fl,dose}$ and $k^{MC}_{fl,fluence}$) by a factor $F(d)$ which takes values from 0.99 to 1.00 at depth.

5. CONCLUSIONS

In this work, fluence correction factors to convert absorbed dose to graphite to absorbed dose to water were determined for graphite calorimetry. Measurements were performed with a 60 MeV energy beam at CCC, and an 180 MeV at the PTC Czech and compared with Monte Carlo simulations. A mathematical formalism was presented which relates fluence corrections derived by numerical simulations using the FLUKA Monte Carlo code[1,2] to partial fluence corrections determined experimentally.

Fluence corrections calculated by experiments are partial because they account for differences in the primary and part of the secondary particles' fluence. A correction factor, $F(d)$, was established to relate fluence corrections as defined by theory and partial fluence corrections derived by experiment. For the PTC Czech beam, fluence corrections increased from 0.99 to 1.04 with depth. For the CCC beam, the magnitude of the fluence correction factor was approximately 0.99 at all depths when derived in an area equal to the sensitive area of the chamber used in the experiments. A larger area was also considered to study the contribution of particles that scatter outside the effective area of the chamber and fluence corrections were found to increase from 0.99 toward 1.01 in depth.

The results are relevant to the use of water and tissue-equivalent-plastic materials in the clinic given their carbon content. The work presented here is a first step for the conversion between dose to graphite to dose to water in low- and high-energy proton beams. This work will also contribute to improved absolute proton dosimetry using a graphite calorimeter and its establishment as a primary standard.

ACKNOWLEDGMENTS

The authors would like to thank David Shipley and Sebastian Galer for all the support with Monte Carlo simulations and Michael Homer and Nigel Lee for their assistance during the experiments. The authors also wish to thank Tania Avgoulea for proofreading the paper. The authors acknowledge the use of the UCL Legion High Performance Computing Facility (Legion@UCL), and associated support services, in the completion of this work, and the FLUKA mailing list for all the support with FLUKA code. A.L. was supported by NPL and EPSRC.

CONFLICT OF INTEREST DISCLOSURE

The authors declare that there is no conflict of interest.

[a]Author to whom correspondence should be addressed. Electronic mail: am.lourenco@ucl.ac.uk

[1]A. Ferrari, P. R. Sala, A. Fassó, and J. Ranft, "FLUKA: A multi-particle transport code," CERN 2005-10, INFN/TC 05/11, SLAC-R-773 (2005).
[2]T. T. Böhlen, F. Cerutti, M. P. W. Chin, A. Fassó, A. Ferrari, P. G. Ortega, A. Mairani, P. R. Sala, G. Smirnov, and V. Vlachoudis, "The FLUKA code: Developments and challenges for high energy and medical applications," Nucl. Data Sheets **120**, 211–214 (2014).
[3]ICRU, "Prescribing, recording, and reporting proton-beam therapy," Report 78, Bethesda, MD, 2007.
[4]IAEA, "Absorbed dose determination in external beam radiotherapy: An international code of practice for dosimetry based on standards of absorbed dose to water," Technical Report Series TRS-398, 2000.
[5]H. Palmans, M. Bailey, S. Duane, D. Shipley, and R. Thomas, "Development of a primary standard level proton calorimeter at NPL," Radiother. Oncol. **84**(Suppl. 1), S135 (2007).
[6]H. Palmans, R. Thomas, M. Simon, S. Duane, A. Kacperek, A. DuSautoy, and F. Verhaegen, "A small-body portable graphite calorimeter for dosimetry in low-energy clinical proton beams," Phys. Med. Biol. **49**, 3737–3749 (2004).
[7]AAPM, "Protocol for heavy charged-particle therapy beam dosimetry; a report of Task Group 20 Radiation Therapy Committee, American Association of Physicists in Medicine Report 16," American Institute of Physics (1986).
[8]S. Vynckier, D. E. Bonnett, and D. T. L. Jones, "Code of practice for clinical proton dosimetry," Radiother. Oncol. **20**, 53–63 (1991).
[9]S. Vynckier, D. E. Bonnett, and D. T. Jones, "Supplement to the code of practice for clinical proton dosimetry," Radiother. Oncol. **32**, 174–179 (1994).
[10]ICRU, Clinical proton dosimetry. I. Beam production, beam delivery and measurement of absorbed dose (Report 59) IAEA TRS-398, 1998.
[11]H. Paganetti, "Nuclear interactions in proton therapy: Dose and relative biological effect distributions originating from primary and secondary particles," Phys. Med. Biol. **47**, 747–764 (2002).
[12]H. Palmans, L. Al-Sulaiti, P. Andreo, D. Shipley, A. Lühr, N. Bassler, J. Martinkovič, J. Dobrovodský, S. Rossomme, R. A. S. Thomas, and A. Kacperek, "Fluence correction factors for graphite calorimetry in a low-energy clinical proton beam. I. Analytical and Monte Carlo simulations," Phys. Med. Biol. **58**, 3481–3499 (2013).
[13]A. Lühr, D. C. Hansen, N. Sobolevsky, H. Palmans, S. Rossomme, and N. Bassler, "Fluence correction factors and stopping power ratios for clinical ion beams," Acta Oncol. **50**, 797–805 (2011).
[14]S. Rossomme, H. Palmans, D. Shipley, R. Thomas, N. Lee, F. Romano, P. Cirrone, G. Cuttone, D. Bertrand, and S. Vynckier, "Conversion from dose-to-graphite to dose-to-water in an 80 MeV/A carbon ion beam," Phys. Med. Biol. **58**, 5363–5380 (2013).
[15]H. Palmans, L. Al-Sulaiti, P. Andreo, R. A. S. Thomas, D. R. S. Shipley, J. Martinkovič, and A. Kacperek, "Conversion of dose-to-graphite to dose-to-water in a clinical proton beam," in *Standards, Applications and Quality Assurance in Medical Radiation Dosimetry–Proceedings of an International Symposium* (IAEA, Vienna, Austria, 2011), Vol. 1, pp. 343–355.
[16]G. X. Ding, D. W. Rogers, J. E. Cygler, and T. R. Mackie, "Electron fluence correction factors for conversion of dose in plastic to dose in water," Med. Phys. **24**, 161–176 (1997).
[17]K. R. Kase, G. J. Adler, and B. E. Bjärngard, "Comparisons of electron beam dose measurements in water and polystyrene using various dosimeters," Med. Phys. **9**, 13–19 (1982).
[18]D. I. Thwaites, "Measurements of ionisation in water, polystyrene and a 'solid water' phantom material for electron beams," Phys. Med. Biol. **30**, 41–53 (1985).
[19]H. Palmans, J. E. Symons, J. M. Denis, E. A. Kock, D. T. L. Jones, and S. Vynckier, "Fluence correction factors in plastic phantoms for clinical proton beams," Phys. Med. Biol. **47**, 3055–3071 (2002).
[20]*Proton Therapy Physics*, edited by H. Paganetti, Series in Medical Physics and Biomedical Engineering (CRC, Florida, 2011).
[21]ICRU, "Stopping powers and ranges for protons and alpha particles," Report 49, Bethesda, MD, 1993.
[22]C. Gomà, P. Andreo, and J. Sempau, "Spencer-Attix water/medium stopping-power ratios for the dosimetry of proton pencil beams," Phys. Med. Biol. **58**, 2509–2522 (2013).
[23]F. Verhaegen and H. Palmans, "A systematic Monte Carlo study of secondary electron fluence perturbation in clinical proton beams (70–250 MeV) for cylindrical and spherical ion chambers," Med. Phys. **28**, 2088–2095 (2001).
[24]G. Grosswendt and W. Y. Baek, "W values and radial dose distributions for protons in TE-gas and air at energies up to 500 MeV," Phys. Med. Biol. **43**, 325–337 (1998).
[25]ICRU, "Nuclear data for neutron and proton radiotherapy and for radiation protection," Report 63, Bethesda, MD, 2000.
[26]D. E. Bonnett, A. Kacperek, M. A. Sheen, R. Goodall, and T. E. Saxton, "The 62 MeV proton beam for the treatment of ocular melanoma at Clatterbridge," Br. J. Radiol. **66**, 907–914 (1993).
[27]C. Baker, D. Shipley, H. Palmans, and A. Kacperek, "Monte Carlo modelling of a clinical proton beam-line for the treatment of ocular tumours," Nucl. Instrum. Methods Phys. Res., Sect. A **562**, 1005–1008 (2006).
[28]A. Kacperek, "Protontherapy of eye tumours in the UK: A review of treatment at Clatterbridge," Appl. Radiat. Isot. **67**, 378–386 (2009).
[29]ISO, *Guide to the Expression of Uncertainty in Measurement* (International Organization for Standardization (ISO), Geneva, 1995).
[30]M. Schippers, in *Proton Beam Production and Dose Delivery Techniques - Principles and Practice of Proton Beam Therapy (AAPM 2015 Summer School)*, edited by I. J. Das and H. Paganetti (Medical Physics Publishing, Madison, WI, USA, 2015).